Probabilistic Prediction of Postdisaster Functionality Loss of Community Building Portfolios Considering Utility Disruptions

Weili Zhang[1]; Peihui Lin[2]; Naiyu Wang, A.M.ASCE[3]; Charles Nicholson[4]; and Xianwu Xue[5]

Abstract: This study proposes a framework for the probabilistic prediction of building portfolio functionality loss (BPFL) in a community following an earthquake hazard. Building functionality is jointly affected by both the structural integrity of the building itself and the availability of critical utilities. To this end, the framework incorporates three analyses for a given earthquake scenario: (1) evaluation of the spatial distribution of physical damages to both buildings and utility infrastructure; (2) computation of utility disruptions deriving from the cascading failures occurring in interdependent utility networks; and (3) by integrating the results from the first two analyses, making a probabilistic prediction of the postevent functionality loss of building portfolios at the community scale. The framework couples the functionality analyses of physical systems of distinct topologies and hazard response characteristics in a consistent spatial scale, providing a rich array of information for community hazard mitigation and resilience planning. An implementation of the BPFL framework is illustrated using the residential building portfolio in Shelby County, Tennessee, subjected to an earthquake hazard. **DOI: 10.1061/(ASCE)ST.1943-541X.0001984.**

Author keywords: Community resilience; Building functionality loss; Physical infrastructure; Interdependent utility networks; Uncertainty modeling; Earthquake hazard.

Introduction

Communities are highly dependent on the functionality of their physical infrastructure to deliver essential services, provide shelter, and support socioeconomic interests. Essential to the built environment are the wide array of buildings in the community (building portfolio) and the critical utility systems (e.g., electric power and water). Research with respect to enhancing community resilience to hazards is an active and ongoing area of investigation (Bruneau et al. 2003; Chang and Shinozuka 2004; Dueñas-Osorio et al. 2007; Bocchini and Frangopol 2012; Lounis and McAllister 2016). Pioneering community leaders in San Francisco (Poland 2013), Oregon (OSSPAC 2013), and other areas have outlined plans and goals to improve community resilience to natural hazards. Among these efforts, there is an increasing demand for a quantitative approach to predict the building portfolio functionality loss (BPFL) at a community scale. Substantial BPFL following a hazard undermines fundamental community functions such as housing, education, commerce, and government. This, in turn, may lead to significant economic and social consequences, including population dislocation, business closures, and increased unemployment. A realistic and quantitative estimate of the probabilistic spatial distribution of BPFL for a community can provide vital information for decision support to community leaders regarding both disaster mitigation and recovery planning (e.g., estimate the number and locations of temporary shelter needs, allocate health care resources for efficient postdisaster rescue, planning for emergency drinking-water supply, etc.).

Building portfolios are one of the most complex physical systems in a community because they, on one hand, serve as the receiving end of all utility networks and, on the other hand, directly interface with the population (Lin and Wang 2017a, b). Functionality of an individual building can be defined as its availability to be used for its intended purpose, which is a function of its structural integrity and availability of utilities (Almufti and Willford 2013). A main cause of building functionality loss is hazard-induced structural or nonstructural damages because a building relies on its load-resistant system to provide safety and on its nonstructural components (e.g., lighting, heating, elevators, etc.) to provide serviceability. Another primary cause of building functionality loss is the disruption of basic utilities, i.e., an undamaged building is not functional if certain utilities (such as water and power) are unavailable. To the best of the authors' knowledge, building functionality loss prediction at a community scale based on a fully coupled building profile and utility networks has not been studied in the literature.

Buildings can be considered as the demand nodes of utility networks. To explicitly consider the availability of critical utilities to meet the demand of a building portfolio, a network model that can capture the interdependent nature among utilities is required. Among existing classifications of different types of interdependency between infrastructure networks (cf. Ouyang 2014), the four classes categorized by Rinaldi et al. (2001) are well accepted: (1) physical (i.e., functionality of one infrastructure network

[1]Graduate Research Assistant, Dept. of Industrial and Systems Engineering, Univ. of Oklahoma, Norman, OK 73019.

[2]Graduate Research Assistant, School of Civil Engineering and Environmental Science, Univ. of Oklahoma, Norman, OK 73019.

[3]Assistant Professor, School of Civil Engineering and Environmental Science, Univ. of Oklahoma, Norman, OK 73019 (corresponding author). E-mail: naiyu.wang@ou.edu

[4]Assistant Professor, Dept. of Industrial and Systems Engineering, Univ. of Oklahoma, Norman, OK 73019.

[5]Postdoctoral Research Fellow, School of Civil Engineering and Environmental Science, Univ. of Oklahoma, Norman, OK 73019.

Note. This manuscript was submitted on November 2, 2016; approved on September 7, 2017; published online on January 19, 2018. Discussion period open until June 19, 2018; separate discussions must be submitted for individual papers. This paper is part of the ***Journal of Structural Engineering***, © ASCE, ISSN 0733-9445.

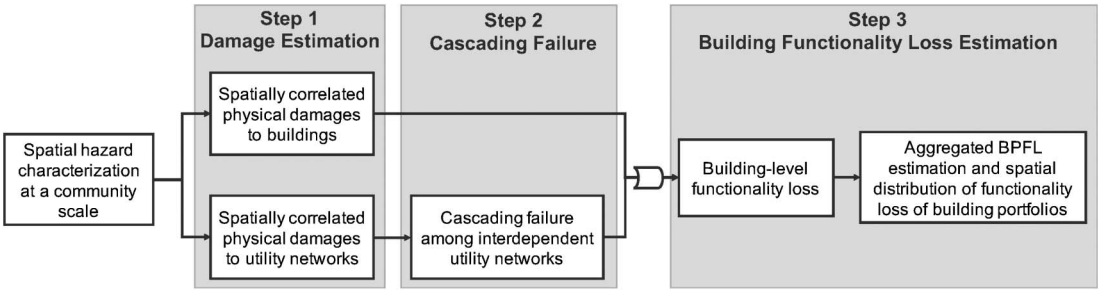

Fig. 1. Flowchart for building portfolio functionality loss estimation

depends on the physical input of another); (2) cyber (i.e., the state of one infrastructure network depends on the information flow of another); (3) geographic (i.e., two components are colocated); and (4) logical (i.e., types of dependency that are not physical, cyber, or geographic). A variety of approaches have been proposed to model such interdependencies, including (1) empirical-based analyses; (2) agent-based models; (3) input-output models; and (4) network flow approaches. Empirical-based analyses make use of historical data of given disasters to identify failure patterns (Mendonça and Wallace 2006; Luiijf et al. 2008; Utne et al. 2011). The data used in such model development are often both location-specific and hazard-specific and cannot be generalized. Agent-based approaches model interdependent networks as complex adaptive systems in which the network components are agents that interact within a virtual environment based on predefined rules (Dudenhoeffer et al. 2006). Agent-based models require many assumptions to define the agent-specific rules, which can be difficult to calibrate and validate because of a lack of data. The Leontief input-output model has been widely studied and successfully applied to interdependent lifelines to measure economic relationships among infrastructure sectors (Haimes and Jiang 2001; Santos and Haimes 2004; Haimes et al. 2005a, b; Xu et al. 2011). However, it is not suitable for analyzing dependencies at high levels of granularity such as the infrastructure component–level. Network flow–based interdependency models provide a direct representation of lifeline infrastructure systems (e.g., electric power network, water distribution networks, gasline distribution networks) and their interdependences using graphs composed of nodes and arcs (Lee et al. 2007; Ouyang and Dueñas-Osorio 2011; Trucco et al. 2012; González et al. 2016). Network flow models readily handle many layers of networks, multiple commodities, and a wide variety of interdependency relationships. Furthermore, such models naturally support the component-level resolution necessary for coupling individual buildings as demand nodes with specific elements of the utility networks and are applicable to various communities of different sizes and topologies.

This study proposes a BPFL estimation framework that integrates three analysis steps, as shown in Fig. 1. Damage estimation is used to evaluate the spatial distribution of physical damages to both buildings and utility networks for a given earthquake scenario. The uncertainties in the spatially varying hazard demands and structural capacities, as well as the spatial correlations among these variables, are modeled and propagated throughout the analysis. Cascading failure analysis is used to compute the functionally-interdependent utility disruptions from cascading failures by using a state-of-the-art network flow–based model of the interdependent utility networks. Lastly, building functionality loss estimation is used to integrate the physical damage to buildings with utility disruptions to quantify the aggregated BPFL at a community scale as well as the spatial variation in the functionality loss across the geographic domain of the community. The framework couples the functionality analyses of physical systems of distinct topologies and hazard response characteristics in a consistent spatial scale, providing a rich array of quantitative information for hazard mitigation and resilience planning. The researchers emphasize that the current work only focuses on BPFL immediately following an earthquake event, which is the necessary starting point for the critical next step of modeling the temporal evolution of building portfolio functionality recovery. In the remainder of this study, the authors first discuss the overall framework and mathematical formulation, then illustrate the proposed methodology using Shelby County, Tennessee as a testbed and finally provide concluding remarks.

Framework to Assess Functionality Loss of Community Building Portfolios

Definition of Building Functionality

This study adopts the definition of building functionality proposed by Almufti and Willford (2013), in which building functionality is defined as the building's capacity to be used for its intended purpose, depending on (1) its structural integrity to provide shelter, and (2) utility availabilities at the building site. In an earthquake hazard, based on the degree of structural, nonstructural or other type of damage to a building following an earthquake, its functionality is generally categorized into three levels: restricted entry (red placard), restricted use (yellow placard), and reoccupancy (green placard) (Oaks 1990). Only buildings tagged with green placards are safe to occupy. In addition to the safety requirement, utilities (water, power, gas, etc.) need to be available for a building to be functional. Accordingly, five different states of building functionality are defined in Table 1, ranging from restricted entry to full functionality. Each functionality state corresponds to a unique combination of a building's physical damage condition and its utility availability. Detailed discussions on the classification of building functionality states can be found in literature (Almufti and Willford 2013; Lin and Wang 2017a, b). For simplicity, building functionality in this study is generalized into two broad categories: functional (States 4 and 5) and nonfunctional (States 1–3). Accordingly, there are three major steps to estimate BPFL as illustrated in Fig. 1, which are discussed in detail in the subsequent sections, respectively.

Damage Assessment of Buildings and Utility Networks

An earthquake scenario, S_{EQ}, is often characterized by a specific magnitude M_w and an epicenter distance D from a site of interest. The appropriate scenario event for resilience assessment of a community should be identified based on the hazard frequency analysis and the risk tolerance of the specific community under

Table 1. Building Functionality States under Earthquake Hazard

Identifier	Functional states	Building damage description	Utilities accessibility	Functionality category
1	Restricted entry	Extensive structural and nonstructural damage; unsafe to occupy or enter	N/A	Nonfunctional
2	Restricted use	Moderate to extensive structural and nonstructural damage; portion of the building is unsafe to occupy	N/A	
3	Reoccupancy	Minor to moderate structural and nonstructural damage; safe enough to be used for shelter	N/A	
4	Baseline functionality	Minor cosmetic structural and nonstructural damage	Partially available	Functional
5	Full functionality	Minor damage to none	Fully available	

investigation (NIST 2015). With a selected scenario earthquake, the seismic intensity at the specific site of a structure can be obtained subsequently from ground-motion attenuation functions (Atkinson and Boore 1995; Campbell 2003; Atkinson and Boore 2006). Generally, the ground-shaking intensities (IM) are represented by a median acceleration (or velocity) response and period-dependent dispersions

$$\ln(IM_i) = \ln(\overline{IM_i}) + \tau \cdot \xi_i \tag{1}$$

where $\overline{IM_i}$ = expected value of ground-motion intensity at structure site i computed from a selected ground-motion attenuation model; ξ_i = error term often described by a standard normal distribution; and τ = standard deviation of $\ln(IM_i)$.

The joint probability of ground-motion intensity at all structure sites is a multivariate lognormal distribution. For any two structures within the same community, their seismic intensities are positively correlated because the common hazard with large footprint, which is often simulated as a random field characterized by an exponentially decayed spatial correlation with respect to the separation distance between the two sites (Goda and Hong 2008; Jayaram and Baker 2009). For this study, the correlation function determined by Wang and Takada (2005) is adopted

$$\rho_{i,j}^{IM} = \exp\left(-\frac{r_{ij}}{R}\right) \tag{2}$$

where r_{ij} = separation distance between structures i and j; and R = correlation distance, typically ranging from 20 to 40 km depending on the hazard characteristics and local site conditions (Wang and Takada 2005).

For buildings and engineered utility facilities in the community, damage states are often estimated using fragility functions, which express the probability that the response of a structural system equals or exceeds a stipulated damage state as a function of hazard intensity. Lognormal probability distributions are commonly assumed (FEMA/NIBS 2003)

$$\mathrm{P}[ds|IM] = \Phi[\ln(IM/\overline{IM}_{ds})/\beta_{ds}] \tag{3}$$

where $\overline{IM}_{ds}$ = median value of seismic intensity IM at which the structure reaches the damage state (ds); and β_{ds} = logarithmic standard deviation of the seismic intensity with respect to ds.

Different intensity measures are often used for different type of structures; spectral displacement (S_d) or spectral acceleration (S_a) are often used as the seismic-intensity measure for buildings, whereas peak ground acceleration (PGA) or peak ground velocity (PGV) are most often used for lifeline components and systems. The ds are described as slight, moderate, extensive, and complete, each being associated with a set of predefined quantitative performance thresholds (in terms of relevant structural response parameters, e.g., interstory draft ratio) (FEMA/NIBS 2003; Steelman et al. 2007). Eq. (3) computes the discrete probabilities of these damage states for buildings and individually engineered utility facilities including gate stations and substations in power networks and water tanks and pumping stations in water networks.

For distributed line segments, such as buried water or gas pipelines, the number of breaks (N) in a pipeline segment of length L conditional on given seismic intensity (PGV) can be modeled by a Poisson distribution (Adachi and Ellingwood 2008)

$$\mathrm{P}[N = n] = e^{-\gamma L}\frac{(\gamma L)^n}{n!} \tag{4}$$

Accordingly, the failure probability of the pipe segment is

$$P_{f,pipe} = 1 - \mathrm{P}[N = 0] = 1 - e^{-\gamma L} \tag{5}$$

where γ = pipe-break rate, which is generally assumed to be 20% of pipe-break density, RR, which in turn can be estimated by the following empirical formula (Dueñas-Osorio et al. 2007):

$$RR = 0.0001 \times \mathrm{PGV}^{2.25} \tag{6}$$

where RR is expressed in terms of the number of breaks per-unit kilometer, and the unit of seismic intensity PGV is centimeters per second.

Cascading Failures of Interdependent Utility Networks

To model the complete utility disruption at building sites resulting from failures in utility networks, this study introduces the following network flow model. The cascading failures in interdependent networks model (CFIN) takes as inputs the list of all components that have been directly damaged because of the hazard and are no longer functional (e.g., a list of nonfunctional substations, etc.) and computes the indirect cascading effects as the utility disruption logically propagates throughout the community. For instance, if an electric power network (EPN) component is destroyed (an input to the model), then the resulting power outage may render a nearby water pumping station inoperable (an output of the model). This water disruption may impact residential buildings further away that still have power (an output of the model). The CFIN model introduced herein is based on the interdependent network design proposed by Lee et al. (2007) and improved by González et al. (2016), but has been revised in the present study with a focus on quantifying the cascading failures among interdependent networks conditioned on the physical damages to the network components discussed previously. The CFIN model differs from those of Lee et al. (2007) and González et al. (2016) in that it does not integrate restoration decision optimization. This simplification improves the efficiency of the approach for the BPFL framework.

The CFIN model can be described mathematically as follows. Let K denote the set of all utility infrastructures (water, EPN, gas, etc.) in the community. Each utility infrastructure $k \in K$ is then described as a network consisting of nodes V^k (e.g., water pumps) and

arcs A^k (e.g., water pipelines) for each infrastructure type. Let L^k denote the set of commodities in infrastructure $k \in K$. A commodity in the CFIN, for example, could be electric power in the EPN or water in the potable-water network (PWN). The sets of nodes modeled as supply, demand, and transshipment nodes are denoted as V_l^{k+}, V_l^{k-}, and $V_l^{k=}$, respectively. The set V_l^{k+} includes the network components that provide commodities to the community, such as the gate stations in the EPN and water tanks in the PWN. The demand nodes V_l^{k-} represent the population needs within the community and may include, for example, substations in the EPN or water distribution points in the PWN. The set $V_l^{k=}$ are nodes used to represent junction points in the network. Let r_i^{lk} denote the amount of the requirements of node $i \in V^k$ for commodity $l \in L^k$ in network $k \in K$. If $r_i^{lk} > 0$, the node is a supply node and the value represents the amount of the associated commodity which is readily available. If $r_i^{lk} < 0$, then node i is a demand node and the value represents the community need at that node (e.g., power needs at a substation or water at a distribution node). If $r_i^{lk} = 0$, then node i is a transshipment node.

The cost of transmitting commodity $l \in L^k$ on arc $(i, j) \in A^k$ is defined as c_{ij}^{lk}. For the EPN, this is the power transmission cost through the network. Let m_i^{lk+} and m_i^{lk-} denote the unit cost of surplus and deficit supply of commodity $l \in L^k$ at node $i \in V^k$. That is, a per-unit cost is assumed if a commodity is unable to be routed through the network to meet demand. Each node and arc have capacities that are denoted by u_i^k and u_{ij}^k, respectively. Let w_i^k denote the failure cost of node $i \in V^k$ in infrastructure $k \in K$.

Of the four types of interdependency, this study specifically models functional interdependency because it is most relevant to the investigated problem. Let $C_{ik}^{\acute{k}}$ denote the set of nodes in network $\acute{k} \neq k$ that node $i \in V^k$ depends upon. For example, if infrastructure k and $\acute{k}$ correspond to the PWN and EPN, respectively, and node i is a particular water pump, then $C_{ik}^{\acute{k}}$ contains all of the components in the EPN that provide power to that pump. $C_{ik}^{\acute{k}}$ can be referred to as the set of parent nodes in $V^{\acute{k}}$ for child node $i \in V^k$. The parent-child relationships handled by the model can be limited to one-way dependencies (e.g., components in the PWN depend on components in the EPN) as well as true interdependencies (e.g., additionally, components in the EPN depend on components in the PWN).

Let the parameter $0 < \lambda_{ik}^{j\acute{k}} \leq 1$ be used to reflect the dependency relationship between child node $i \in V^k$ in network $k \in K$ and parent node $j \in C_{ik}^{\acute{k}}$. This value represents the contribution of the parent node to the functionality of the child node. For example, if child node i is functional when at least one parent node j is functional, then $\lambda_{ik}^{j\acute{k}}$ is set to a value of 1 for all $j \in C_{ik}^{\acute{k}}$. That is, each parent node is alone sufficient for the functionality of node i. As such, this parameter allows for modeling redundancy across the utility networks (e.g., a water pump might depend on the functionality of a generator or a backup generator). On the other hand, if the functionality of node i requires all parent nodes to be functional, then $\lambda_{ik}^{j\acute{k}}$ is set to $1/|C_{ik}^{\acute{k}}|$ for each $j \in C_{ik}^{\acute{k}}$. Consequently, many types of dependency can be represented mathematically by adjusting the value of $\lambda_{ik}^{j\acute{k}}$. This parameter is used in Eq. (15) in the mathematical description of the CFIN model.

Let d_i^k and d_{ij}^k denote the binary functionality states of node $i \in V^k$ and arc $(i, j) \in A^k$, respectively. These parameters are set to 1 if the corresponding node or arc are rendered nonfunctional by a hazard; otherwise, they are set to 0. These parameter inputs are computed from Step 1 in Fig. 1 as described in the previous section.

There are three types of decision variables in the model: flow variables, slack variables, and failure status variables. Let x_{ij}^{lk} denote the flow variable for commodity $l \in L^k$ through arc $(i, j) \in A^k$ in network $k \in K$. Let s_i^{lk+} and s_i^{lk-} denote slack variables to indicate the surplus and deficit of commodity $l \in L^k$ at node i, respectively. Let the binary variable f_i^k take on a value of 1 if node $i \in V^k$ in network $k \in K$ has failed; otherwise, 0. This failure can occur as a result of three causes: (1) direct damage from the hazard; (2) insufficient supply of a required commodity (e.g., electrical power, water, etc.); or (3) failures within the set of parent nodes on which it depends. The CFIN model is proposed in Eqs. (7)–(18)

Minimize

$$\sum_{k\in k}\sum_{l\in L^k}\sum_{(i,j)\in A^k} c_{ij}^{lk}x_{ij}^{lk} + \sum_{k\in k}\sum_{l\in L^k}\sum_{i\in V^{k-},V^{k+}} (m_i^{lk-}s_i^{lk-} + m_i^{lk+}s_i^{lk+}) + \sum_{k\in k}\sum_{i\in V^k} w_i^k f_i^k \tag{7}$$

such that

$$\sum_{(i,j)\in A^k} x_{ij}^{lk} - \sum_{(j,i)\in A^k} x_{ji}^{lk} = r_i^{lk} - s_i^{lk+} + s_i^{lk-}, \quad \forall\ i \in V^{k+} \cap V^{k-}, \quad \forall\ l \in L^k, \quad \forall\ k \in K \tag{8}$$

$$\sum_{(i,j)\in A^k} x_{ij}^{lk} - \sum_{(j,i)\in A^k} x_{ji}^{lk} = 0, \quad \forall\ i \in V^{k=}, \quad \forall\ l \in L^k, \quad \forall\ k \in K \tag{9}$$

$$f_i^k \geq d_i^k, \quad \forall\ i \in V^k, \quad \forall\ k \in K \tag{10}$$

$$Mf_i^k \geq \sum_{l\in L_k} s_i^{lk-}, \quad \forall\ i \in V^{k-} \cup V^{k+}, \quad \forall\ k \in K \tag{11}$$

$$\sum_{l\in L^k} x_{ij}^{lk} \leq u_{ij}^k(1 - d_{ij}^k), \quad \forall\ (i,j) \in A^k, \quad \forall\ k \in K \tag{12}$$

$$\sum_{(j,i)\in A^k}\sum_{l\in L^k} x_{ji}^{lk} \leq u_i^k(1 - d_i^k), \quad \forall\ i \in V^k, \quad \forall\ k \in K \tag{13}$$

$$\sum_{(i,j)\in A^k}\sum_{l\in L^k} x_{ij}^{lk} \leq u_i^k(1 - f_i^k), \quad \forall\ i \in V^k, \quad \forall\ k \in K \tag{14}$$

$$1 - f_i^k \leq \sum_{j\in C_{ik}^{\acute{k}}} \lambda_{ik}^{j\acute{k}}\left(1 - f_j^{\acute{k}}\right), \quad \forall\ i \in \left\{n \in V^k | C_{nk}^{\acute{k}} \neq \emptyset\right\}, \quad \forall\ k \in K \tag{15}$$

$$x_{ij}^{lk} \geq 0, \quad \forall\ (i,j) \in A^k, \quad \forall\ l \in L^k, \quad \forall\ k \in K \tag{16}$$

$$s_i^{lk+}, s_i^{lk-} \geq 0, \quad \forall\ i \in V^k, \quad \forall\ l \in L^k, \quad \forall\ k \in K \tag{17}$$

$$f_i^k \in \{0, 1\}, \quad \forall\ i \in V^k, \quad \forall\ k \in K \tag{18}$$

The objective function in Eq. (7) consists of minimizing the sum of three components: variable flow cost on each arc, cost of excessive or insufficient supply, and node failure cost. Under normal operation (no physical damage), the objective function should reflect the actual operating costs of flow (e.g., power transmission costs). This is achieved by setting the penalties associated with the slack variables (m_i^{lk+} and m_i^{lk-}) and the failure costs (w_i^k) for node i to

values substantially higher than the variable cost associated with flow (c_{ij}^{lk}) on arc (i, j) of commodity l in network k. Without physical damage in the community, the optimization model would route the commodities through the networks to meet all demands at minimum operating cost. In the case of a hazard, however, it may be impossible to meet the community demand. As such, the commodities will still be routed to minimize cost, but now that the potential failure costs and slack penalties likely outweigh the operational costs, the optimal solution will be one that focuses on minimizing those effects. The penalty values and failure costs can be assigned to prioritize the importance of certain utility services and/or service areas in the community if such information is available. For the present study, the penalties are all set to a constant value, as are the node failure costs.

The constraints in Eq. (8) ensure the flow balance on each supply/demand node. Because of their high cost, the slack variables take on nonzero positive values only when the system is damaged and unbalanced (e.g., insufficient power supply to meet all power demands). For transshipment nodes, the constraints in Eq. (9) ensure that the total inflow is equal to the total outflow of the same commodity. Constraints in Eq. (10) update the failure status of each node based on the initial damage states estimated in the previous step. If a node is nonfunctional because of damage ($d_i^k = 1$), the corresponding failure status is forced to 1 ($f_i^k = 1$).

In this study, a supply/demand node is defined as nonfunctional if the corresponding demand is not fully supplied. This is realized by constraints in Eq. (11): if there is a shortage of a required commodity l for node i (i.e., when $s_i^{lk-} > 0$), then the failure variable is also forced to be 1. The parameter M in Eq. (11) is used to enforce the logical relationship between the node failure status decision variable and the related commodity slack decision variables at the same node. The value for M should be set to a sufficiently large value so as to not artificially inhibit feasibility of optimal solutions. Constraints in Eq. (12) ensure that the total flow of all commodities on each arc cannot exceed the corresponding capacity (which is 0 if the arc is nonfunctional because of direct damage). Constraints in Eq. (13) guarantee that the total flow into a node is less or equal to its capacity and is 0 if it is nonfunctional because of direct hazard damage. Constraints in Eq. (14) ensure that if a node is failed (regardless of the reason), total outflow from this node is 0. Constraints in Eq. (15) propagate the failure statuses from parent nodes to child nodes. Constraint Eqs. (16) and (17) define the flow variables and slack variables as continuous and nonnegative. Finally, variables indicating failure statuses are defined as binary in Eq. (18).

The CFIN model is a mixed binary linear programming problem and can be solved using commercial software. However, the binary decision variables are limited to the identification of failed nodes. Additionally, unlike similar network models (Lee et al. 2007; González et al. 2016) the present study does not incorporate restoration decisions. These two characteristics together result in CFIN fast computation times for moderate-sized problems (e.g., Shelby County, Tennessee). This is an important feature for practical implementations of the BPFL framework in that many hazard realizations should be simulated (and their distinct cascading effects computed) to provide a sensible probabilistic measure.

The output of the CFIN model provides the list of infrastructure nodes that have failed and, for each commodity and demand node in the community (i.e., building), the percentage of demand that can be met in the present damaged state. This information, together with the physical damage estimation of the building portfolio, will be used to determine the total functionality loss of community building portfolios next.

Mapping Building Damage and Utility Disruption to Obtain Building Functionality Loss

If this study considers water (W) and power (P) as the necessary utilities to maintain the functionality of a building, the dependence of functionality state (FS_b) of any building (b) on both utility availability and the robustness of the building itself, can be generalized

$$F_b = S_b \cap F_W \cap F_P$$

$$\overline{F_b} = \overline{S_b} \cup \overline{F_w} \cup \overline{F_P}, \quad \forall\ b \in B \tag{19}$$

where F_b = event that building b maintains functionality (i.e., baseline and full functionality states in Table 1), where building b belongs to community building portfolio B; and S_b = event that the building b remains safe to occupy following the hazard event, which is closely related to building damage state discussed previously. In the subsequent analysis, this study assumes a damage state considered extensive or complete will render a building unsafe to occupy (UO) (i.e., $\overline{S_b}$). A more detailed mapping scheme from the four damage states (for both structural and nonstructural components) to the five-functionality states (Table 1) can be found elsewhere (e.g., Lin and Wang 2017b). F_W and F_P = events that the baseline water and power supply is available at the building site, respectively, where these events are derived from the CFIN results; and $\bar{F}_b$, $\overline{S_b}$, $\overline{F_w}$, and $\overline{F_P}$ = complement of events of F_b, S_b, F_W, and F_P, respectively.

At the community scale, the authors further define the functionality loss ratio (FLR) of a building portfolio as the percentage of buildings in the portfolio that are nonfunctional following a hazard

$$FLR = \frac{1}{|B|}\sum_{b\in B} I_b \tag{20}$$

where $|B|$ = total number of buildings in building portfolio B; and I_b = functionality indicator of any building b

$$I_b = \begin{cases} 0 & FS_b = F_b \\ 1 & FS_b = \overline{F_b} \end{cases}, \quad \forall\ b \in B \tag{21}$$

The probability distribution of FLR can be computed through the law of total probability theorem (Lin and Wang 2016)

$$P(FLR \le z|S_{EQ}) = \int \int_{FLR(\boldsymbol{DS})<z} f_{\boldsymbol{DS}|\boldsymbol{IM}}(\boldsymbol{u}|\boldsymbol{v}) f_{\boldsymbol{IM}|S_{EQ}}(\boldsymbol{v}|S_{EQ})\boldsymbol{dudv} \tag{22}$$

where $f_{IM|S_{EQ}}(v|S_{EQ})$ = joint probability density function of ground-motion intensity IM at all building sites [Eqs. (1) and (2)] conditioned on the scenario event S_{EQ}; $f_{DS|IM}(u|v)$ = joint PDF of damage state DS conditional on IM for all buildings in the portfolio, which can be obtained from fragility functions for different building types in the portfolio; and the FLR for a given damage field, $FLR(DS)$, is obtained using Eqs. (19)–(21). Both IM and DS are vectors, and the dimension of these vectors is consistent with the number of buildings in the considered portfolio. Eq. (22) considers uncertainties and spatial correlations in both hazard demands and structural damages of all buildings in the portfolio and can be approximated using the multilayer Monte Carlo simulation shown in Fig. 2. Eq. (22) estimates the probabilistic distribution of FLR for a scenario event, which implies that the uncertainties in the earthquake occurrence and fault location are not considered.

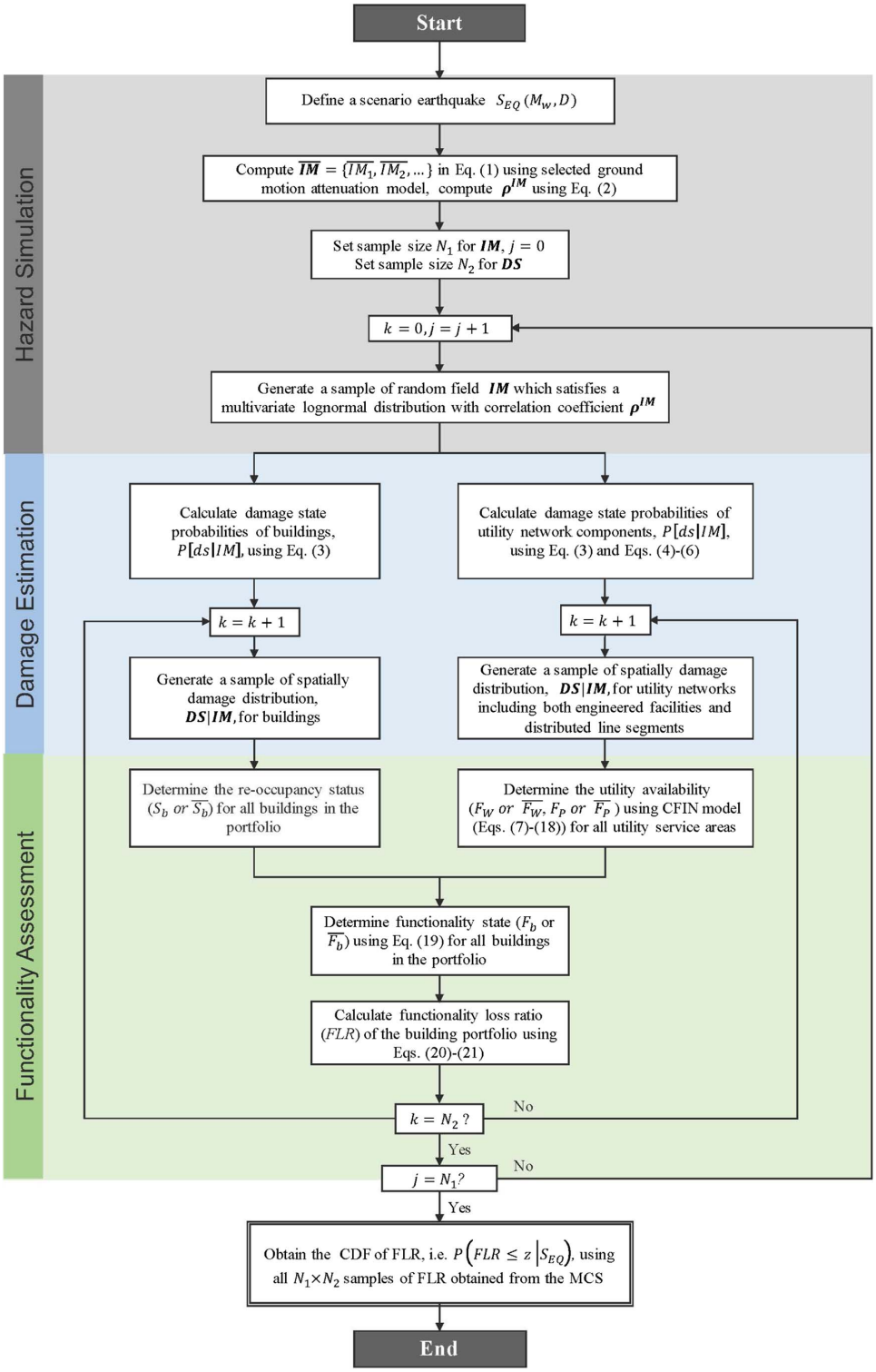

Fig. 2. Multilayer MCS for probabilistic estimation of building portfolio functionality loss for a scenario earthquake

Case Study: Functionality Loss Estimation of the Residential Building Portfolio in Shelby County, Tennessee

Building Portfolio and Utility Networks in Shelby County, Tennessee

The authors now implement the proposed BPFL estimation framework by applying it to the residential building portfolio (RBP) in Shelby County, Tennessee for a likely scenario earthquake. The RBP accounts for approximately 90% of the Shelby building inventory and is distributed spatially across 221 census tracts. Similar to most small and midsized communities in the United States, the RBP in Shelby consists mainly of wood frames. Table 2 summarizes the Shelby RBP by structural types and seismic design code levels, which are consistent with those defined in HAZUS (multi-hazard loss estimation methodology Hazus-MH) (FEMA/NIBS 2003). In particular, the W1 Type wood buildings designed in line

Table 2. Residential Building Portfolio by Structural Type and Seismic Design Code (Data from Steelman et al. 2007)

Structural type[a]	Precode	Low code	Moderate code	High code	Total
C1L	6	21	2	0	29
C1M	4	1	1	0	6
C2H	4	17	8	0	29
C2L	1	1	0	0	2
C2M	0	1	2	0	3
MH	4	32	6	1	43
PC1	0	13	0	1	14
RM1L	0	0	1	0	1
S1H	7	12	6	1	26
S1L	3	286	80	54	423
S1M	0	11	38	25	74
S3	1	4	6	23	34
URML	4,042	3,338	0	0	7,380
URMM	5	0	0	0	5
W1	0	267,958	0	0	267,958
W2	185	4,719	7,166	0	12,070
Total	4,262	276,414	7,316	105	288,097

[a]Description of the structural type: C1 = concrete moment frame; C2 = concrete shear walls; MH = mobile homes; PC1 = precast concrete tilt-up walls; RM1 = reinforced masonry bearing walls with wood or metal deck diaphragms; S1 = steel moment frame; S3 = steel light frame; URM = unreinforced masonry bearing walls; W1 = wood, light frame; W2 = wood, greater than 464.5 m^2 (5,000 ft^2). The character following the abbreviation describing structural type, if present, represents building height class: L = low, M = medium, or H = high.

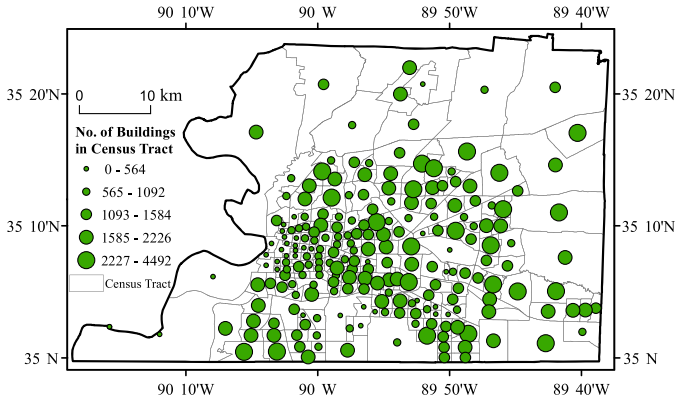

Fig. 3. Distribution of the residential buildings in census tracts of Shelby County (data from Steelman et al. 2007)

with the low seismic code (FEMA/NIBS 2003) account for 93% of the RBP in Shelby. Fragility functions of these building types are adopted from HAZUS for the damage evaluation. Fig. 3 shows the 221 census tracts and associated RBP spatial distribution.

The investigation considers water and power as the critical utilities necessary to maintain the functionality of residential buildings, both of which are managed by the Memphis Light, Gas, and Water (MLGW) Division. Fig. 4 shows the skeletonized topology of the power and water utility systems with major network components. The EPN contains 59 nodes: 8 gate stations, 16 23-kv substations, 21 12-kv substations, and 14 intersections. There are 114 directed arcs representing the power transmission and distribution lines. There is no power plant in Shelby County, and the eight gate stations are considered as supply nodes in the EPN. The EPN intersections are transshipment nodes. The substations are the demand nodes, each of which has a specified electric power service area (EPSA) as indicated in Fig. 4(a). The PWN consists of 49 nodes, including 6 elevated storage tanks, 9 large pumps, and 34 distribution nodes, as well as 98 directed arcs representing water pipeline. The tanks and large pumps are supply nodes and all distribution nodes are demand nodes, each of which has a corresponding potable-water service area (PWSA). In Fig. 4, the number on each node is the node ID, and each arc is identified by the From and To nodes. For instance, the arc (6, 24) in EPN corresponds to the directed arc leaving from the gate station (Node 6) and arriving at the 23-kv substation (Node 24).

Each building in the RBP belongs to a specific EPSA and PWSA based on its geographic location and is supplied with power and water from the respective demand nodes in the corresponding EPSA and PWSA. The total supply capacity and demand of the EPN are 1,434 and 1,003, respectively, representing a 43% reserved capacity. The total supply capacity and demand of the PWN are 1,133 and 997, respectively, representing a 14% surplus (Steelman et al. 2007). Under normal circumstances (e.g., no hazard), both EPN and PWN have more than sufficient supply to meet all the associated demands. These reserved supply capacities provide plausible redundancies to facilitate community emergency response. In this analysis, the authors assume 40% of the full supply of water and power under normal operation conditions represents the utility requirement to maintain the baseline building functionality following a disastrous event.

Fragility functions used to estimate the damage of network components (nodes) in both EPN and PWN are reported in Table 3 (FEMA/NIBS 2003), indicating the EPN components on average are more vulnerable than those in PWN, and the weakest elements in the interdependent EPN-PWN networks are likely to be the gate stations. The failure probability for the PWN pipelines is given in Eqs. (4)–(6). The vulnerability of the EPN transmission lines to earthquake is negligible (Shinozuka et al. 2007) and therefore is not considered for this illustration.

This study assumes that the operation of the pumping stations in PWN fully depends on the input of power from the designated 12- or 23-kv EPN substation in the EPSA in which the pumping station is located. These dependencies are listed in Table 4, showing that each pumping station (third column) depends on the designated substation (first column) in the same row for power input. The CFIN model is assumed that the operating costs, associated with the first term in Eq. (7), are derived from the lengths of the power transmission lines and water pipes. As mentioned previously, the node failure costs and slack penalties are set to values larger than the operating costs. Without having information on node or utility service priorities, this research has set all node failure costs equally and each slack penalty equally. The detailed EPN and PWN data sets can be found in the Mid-America Earthquake Center Seismic Loss Assessment System (MAEViz) database (Steelman et al. 2007) and the Analytics Lab at the OU (IN-CORE 2017). Only one-way dependency is investigated in this case study, i.e., pumping stations depend on the substations for power input; however, the proposed CFIN model can be applied to two-way dependencies in multilayer interdependent networks, as discussed previously.

Analysis and Results

Significant earthquakes in Shelby likely initiate from the New Madrid seismic zone (NMSZ), which consists of three fault segments (New Madrid North, Reelfoot, and Cottonwood Grove). The scenario earthquake with $M_w = 7.7$ and an epicenter located at 35.3 N; 90.3 W used in this study is one of the most likely scenarios

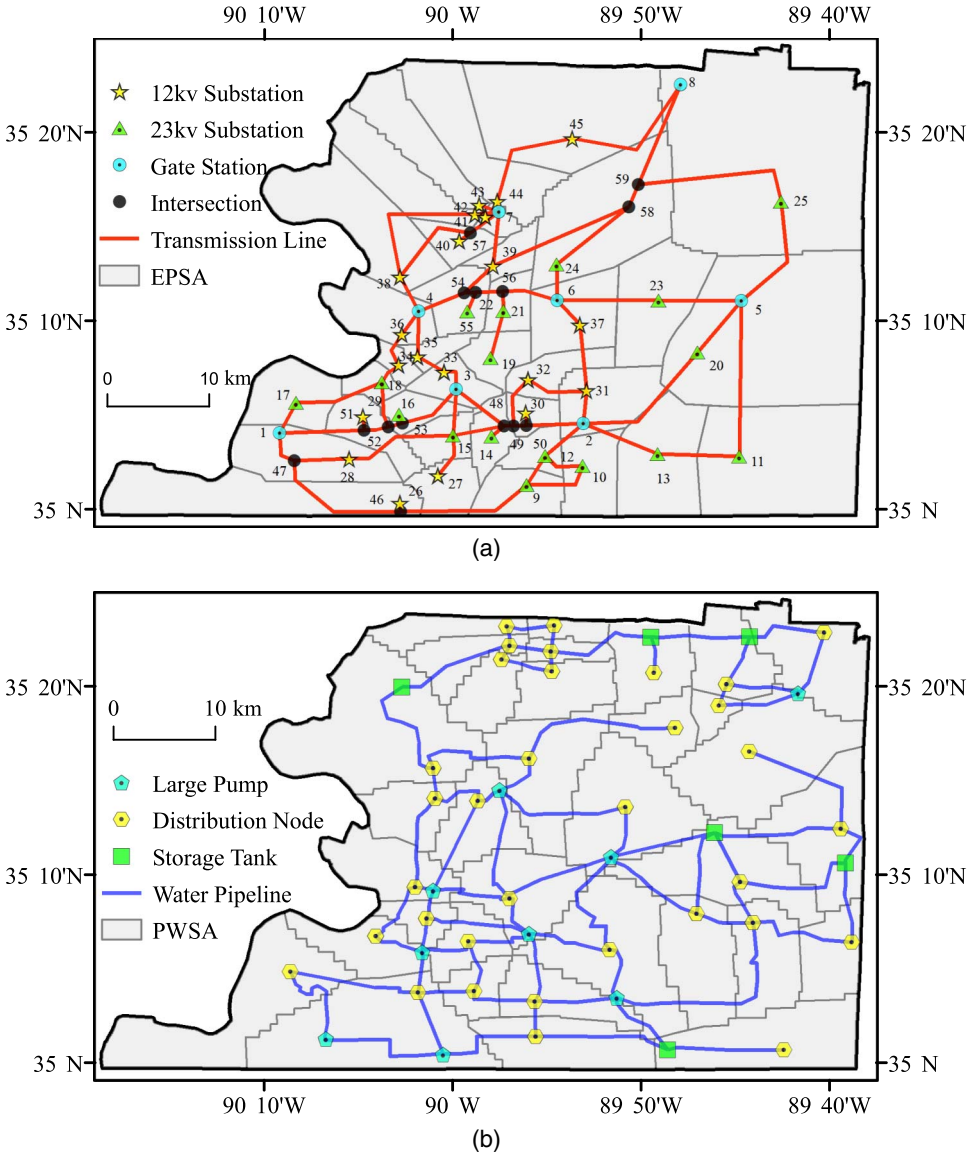

Fig. 4. Skeletonized power and water network topologies in Shelby County, Tennessee: (a) electric power network in Shelby; (b) potable-water network in Shelby

with a 500-year return period based on the disaggregation analysis by United States Geological Survey (2017). Detailed information on soil condition at building sites was unavailable, and the soil was assumed to be Category D over the entire region (Building Seismic Safety Council 2003). The ground-motion attenuation model suggested by Atkinson and Boore (1995) was used for obtaining the spatial seismic-intensity map, which provides both the median seismic intensity (spectral acceleration, PGA, and PGV) shown in Fig. 5 and the variance in the ground motions. The spatial

Table 3. Parameters of Functionality Fragility Functions of Engineered Utility Facilities

Components	Median (g)	β
Gate station	0.47	0.4
23-kv substation	0.7	0.4
12-kv substation	0.9	0.45
Elevated water tank	1.5	0.6
Pumping station	1.5	0.8

Table 4. Functional Dependencies between EPN and PWN

Network	Node	Type
Node in power network (parent node)	10	23-kv substations
	16	23-kv substations
	25	23-kv substations
	27	12-kv substations
	28	12-kv substations
	32	12-kv substations
	36	12-kv substations
	37	12-kv substations
	41	12-kv substations
Node in water network (child node)	4	Large pumps
	5	Large pumps
	12	Large pumps
	2	Large pumps
	3	Large pumps
	6	Large pumps
	8	Large pumps
	9	Large pumps
	39	Large pumps

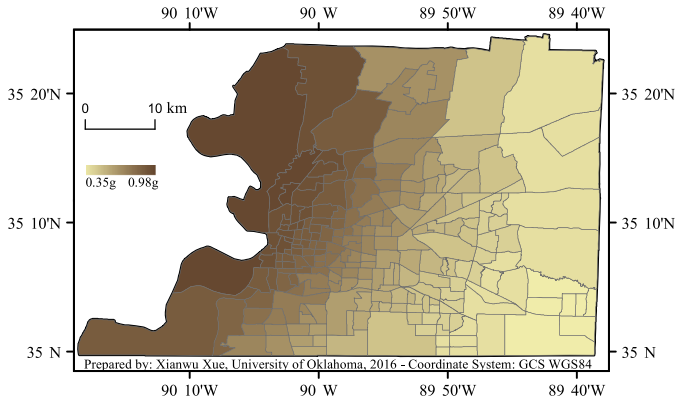

Fig. 5. Median peak ground acceleration with soil amplification

correlation of seismic intensity is modeled, and correlation distance, R, in Eq. (2) is set as 30 km.

The spatially correlated damages to the RBP, EPN, and PWN are first estimated using methodology discussed in the previous section; the cascading failures and the effective water and power distribution are then computed using the CFIN model; finally, the probability of functionality loss at the building level is obtained, and the portfolio-level functionality loss ratio is estimated using Eqs. (19)–(22). To capture the uncertainties in both seismic demand and structural damage resulting from the consider scenario event, the spatially correlated seismic-intensity field is simulated 1,000 times, and conditional on each of these 1,000 demand fields, the resulting physical damages to both buildings and utility networks are simulated for another 1,000 times in the multilayer Monte Carlo simulation (MCS) illustrated in Fig. 2 (i.e., $N_1 = N_2 = 1{,}000$). The $1{,}000 \times 1{,}000$ iterations will result in an unbiased mean estimation of BPFL with 95% confidence with less than 5% relative error.

Fig. 6 shows analysis results from one realization of the demand field in the MCS. Fig. 6(a) displays the spatial distribution of power availability following the scenario event. In this realization of the MCS, four gate stations (3, 6, 7, and 8) and three substations (34, 35, and 42) are physically incapacitated (indicated using lighting symbols). The areas without any power are shaded dark gray, areas with partial supply (40–70% of pre-event demand) are light gray, and the rest of the areas are not affected by the event in terms of power supplies (100% of pre-event demand). The north side of Shelby County is out of power mainly because the damage of Gate Stations 6, 7, and 8. However, because surplus power supply exists in the system, several EPSAs are supplied by alternative gate stations. For example, Substation 41 was originally supplied by Gate Station 7, but is now supplied by Gate Station 4 with 100% of its normal demand following the hazard. The supply redistribution conditional on the network damage is guided by maximizing the power service coverage, i.e., maximizing the number of buildings that are supplied by at least 40% of their pre-event demand. An area in central Shelby County is completely out of power because the failures of Substations 34 and 35. As previously clarified in CFIN model, if a node is damaged, then no commodities (i.e., water or power) can flow through it. Accordingly, Substation 33 is also failed because no path exists from this substation to a functional gate station.

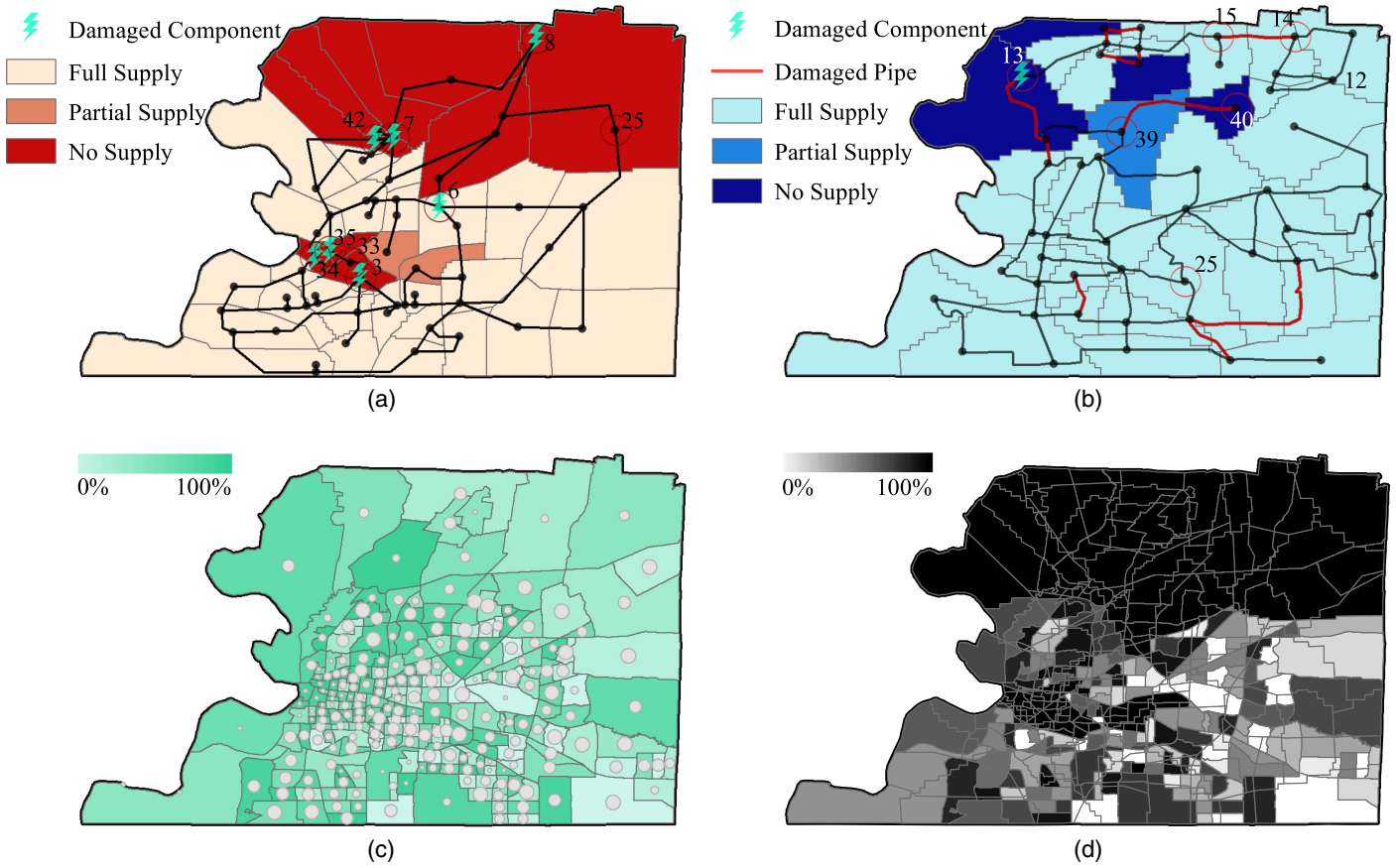

Fig. 6. Functionality loss from one realization of the MCS: (a) area of power outage; (b) area of water outage; (c) percentage of UO buildings; (d) percentage of building functionality loss

The serviceability in PWN shares some similar pattern, but also presents significant differences from that of the EPN. As illustrated in Fig. 6(b), Storage Tank 13 and another 10 pipelines (highlighted in dark gray) are physically damaged. Pumping Station 12 is nonfunctional because of the failure of a parent node (Substation 25). However, no water outage is observed in the northeast broader region of Shelby because the restored water in Tanks 14 and 15 are still functional and sufficient to meet the demand in this region, which shows again that the supply redundancy helps mitigate water outages under abnormal conditions. On the other hand, Water Distribution Node 40 is connected only to Water Node 39 (without alternative supply options); hence, the damage of the pipeline connecting them leads to the water outage in the corresponding PWSA.

Fig. 6(c) shows that the percentage of buildings that are unsafe to occupy (UO) in each census tract ranges from 0 to 84% because of the large variations in the seismic intensities propagated from earthquake epicenter to each building site. Considering the joint effect of the physical damage and utility disruption, the spatial functionality losses of residential buildings are shown in Fig. 6(d). Buildings in considerable numbers of census tracts completely lost their functionality because the absence of water or power despite the fact that the physical damage to building portfolio itself is comparatively minor. For example, a large area on the north side of Shelby suffers from complete power outage, leading to significant functionality losses of the building portfolio in that area immediately following the hazard.

Fig. 7 presents the expected functionality loss ratio for the EPN, PWN, and RBP resulting from the multilayer MCS for the considered scenario event. As depicted in Fig. 7(a), western Shelby is more susceptible to power outages than eastern Shelby because of the failure pattern of the EPN components. This is consistent with the spatial variation of seismic intensity in Fig. 5. The average failure probability of a gate station is approximately 60%; Gate Stations 1, 3, 4, and 7 are the most vulnerable components, especially because they are closer to the earthquake epicenter. On average, 53% of the original demand in Shelby can be satisfied following the considered earthquake scenario. The highest probability of power outage is approximately 77% for the highlighted region at northwest corner of Shelby.

The average ratio of water outage is 41% cross Shelby following the considered scenario, as shown in Fig. 7(b). Unlike the patterns for power outage or building damage, the spatial distribution of water outage does not show a strong correlation with the PGA. This is because in addition to the seismic intensity, PWN failure is also strongly impacted by the water pipeline breaks as well as the cascading effect of power outage at pumping stations. The highest probability of water outage is approximately 80%, as seen in a few areas highlighted in Fig. 7(b). In particular, the failure probabilities of Intersections 36 and 40 are approximately 33%, and there is only one path connecting these intersections with their respective water supply nodes. Therefore, the corresponding PWSAs suffer higher probability of water outage. In addition, the water outage

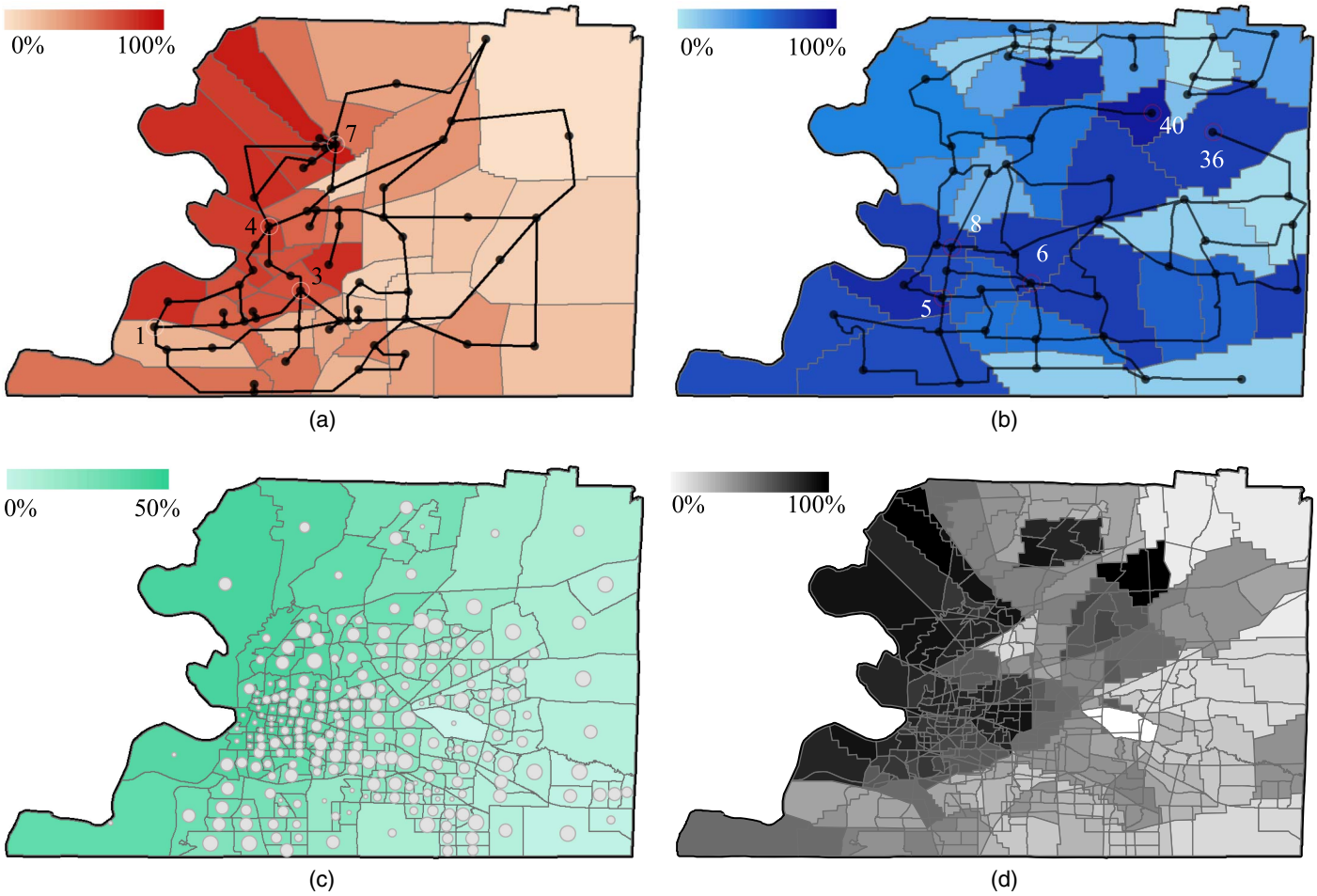

Fig. 7. Functionality loss ratio estimated from the multilayer MCS: (a) ratio of power outage; (b) ratio of water outage; (c) unsafe-to-occupy ratio; (d) building FLR

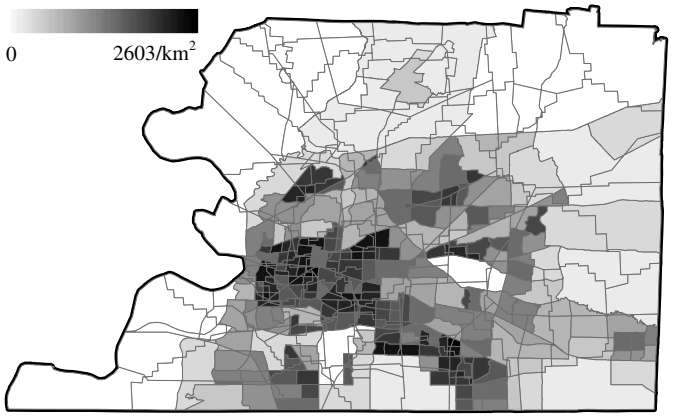

Fig. 8. Densities of affected population in census tracts

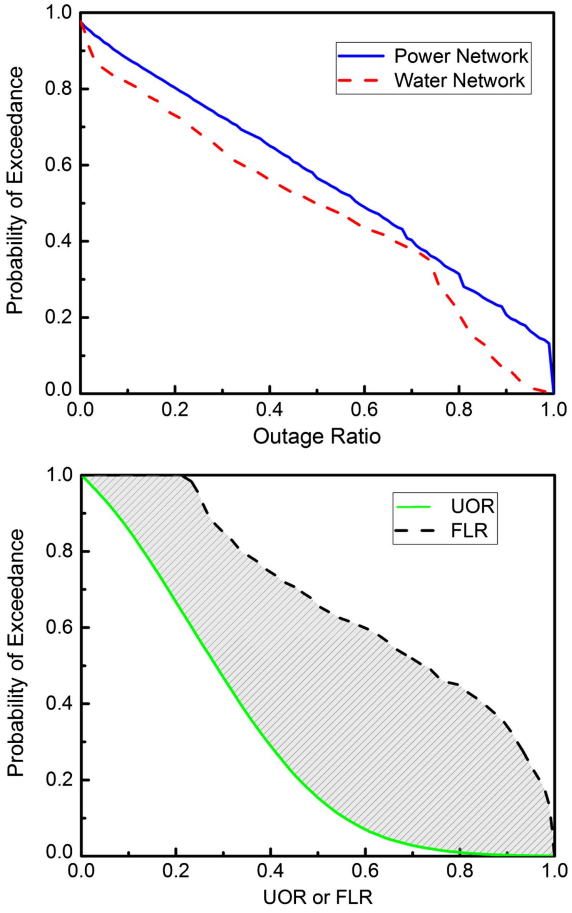

Fig. 9. Exceedance probability of (a) outage ratios of EPN and PWN; (b) UOR and FLR of the RBP

probability in central areas of Shelby is considerably high because (1) there are only three large pumps (5, 6, and 8) in this area and no storage tank close by for redundancy; and (2) these three pumps provide 30% of water supply in Shelby, but the average probability of their failure is as high as 80% for the considered earthquake scenario.

Fig. 7(c) indicates that the expected ratio of UO buildings (UOR) in each census tract, ranges between 13 and 47% from west to east and positively correlates to spatial variation in seismic intensity. This is because the majority of the Shelby RBP is W1 wood structures designed with low seismic performance requirements, making the RBP nearly homogenous in terms of seismic resistance. The spatial distribution of building functionality loss is shown in Fig. 7(d), which clearly reflects both the physical damage to RBP and the service disruption trends in the EPN and PWN. The patterns of functionality loss in RBP, EPN, and PWN, and, more importantly, the quantitative characterization of these patterns, can only be obtained from an estimation framework in which analysis of different physical systems are fully coupled on a consistent spatial scale in a probabilistic manner, as introduced herein.

Fig. 8 depicts the spatial density of the affected population, calculated by multiplying the population density by building functionality loss ratio [cf. Fig. 7(d)] for each census tract. This result correlates to the percentage of residents in each tract who would need to dislocate (at least on a short-term basis) or need temporary shelter. The building FLR is the highest at the northwest corner of Shelby, as shown in Fig. 7(d), but the density of affected population is low there because of sparse residences. Similarly, although the building FLR is moderate in the central portion of Shelby, the affected population density is high because this area is most heavily populated.

Fig. 9(a) presents the aggregated exceedance probability of the EPN and PWN outage ratio (ratio of supply shortage to predisaster demand) for the entire Shelby area, indicating the water and power outage ratio follow approximately uniform distributions. The expected values of water and power outage ratios are 66.39 and 70.92%, respectively. In Fig. 9(b), the UOR and FLR of the Shelby RBP are depicted. The FLR is significantly higher than the UOR, with expected values of 43.7 and 23.8%, respectively. This illustrates that neglecting the impact of utility disruption will result in significant underestimation of building portfolio functionality loss following a hazard event, leading to conservative estimation of the challenges facing the community during emergency response and postdisaster recovery. This BPFL estimation immediately following a disaster provides a starting point for modeling the temporal evolution of building portfolio functionality recovery, which is a critical next step toward resilience planning.

Conclusions

This study introduced a new probabilistic framework to predict the functionality loss of community building portfolios following extreme natural hazard events, in which the functionality loss of a building portfolio is jointly impacted by both the physical damage of buildings and utility disruptions at the building sites. The major attributes of the framework include the following:

- The framework fully couples the functionality analyses of physical systems of distinct topologies and hazard response characteristics on a consistent spatial scale at the community level, providing a physics-based quantitative measure of both the aggregated BPFL ratio and spatial variation in functionality loss across the geographic domain of the community;
- The framework includes a multilayer MCS to propagate the uncertainties and spatial correlations in both hazard-demand and structural-response parameters in each of the involved physical systems throughout the BPFL estimation framework, forming the basis for risk-informed planning decisions;
- The cascading failures among interdependent networks are modeled using the CFIN model—a state-of-the-art network flow–based mixed-integer linear programming model. The study reveals that the cascading effect in utility networks has a significant impact on the BPFL and, more importantly, that

the proposed framework can provide quantitative measures of such an impact. The CFIN model can be effectively applied to predict postevent utility outage ratios for communities with only a minimal input of information regarding the utility network topologies, expected commodity supplies and demands, and network component fragility data. The mathematical model can be implemented with a variety of algebraic modeling languages (e.g., GAMS) or computer programming languages (e.g., Python) and optimized using any mixed-integer linear mathematical programming solver (e.g., *CPLEX* or *Gurobi*); and

- The spatial pattern of BPFL is affected by many factors, including the spatial variation of hazard intensity, the inherent vulnerably of buildings and components of utility systems, the cascading failures in interdependent utility networks, as well as the redistribution of surplus supply capacity in the utility networks. The proposed framework does not merely reveal such nonintuitive spatial patterns, but also effectively quantifies the comprehensive joint impacts, providing rich array of information for hazard mitigation.

Acknowledgments

The research reported herein was supported, in part, by the Center for Risk-Based Community Resilience Planning, funded by the National Institute of Standards and Technology (NIST) under Cooperative Agreement No. 70NANB15H044. This support is gratefully acknowledged. The authors also thank Dr. Leonard Duenas Osorio at Rice University for his helpful advice at early stage of this study. The views expressed are those of the authors, and may not represent the official position of the NIST.

References

Adachi, T., and Ellingwood, B. R. (2008). "Serviceability of earthquake-damaged water systems: Effects of electrical power availability and power backup systems on system vulnerability." *Reliab. Eng. Syst. Saf.*, 93(1), 78–88.

Almufti, I., and Willford, M. (2013). *REDiTM rating system: Resilience-based earthquake design initiative for the next generation of buildings*, ARUP Co., London.

Atkinson, G. M., and Boore, D. M. (1995). "Ground-motion relations for eastern North America." *Bull. Seismol. Soc. Am.*, 85(1), 17–30.

Atkinson, G. M., and Boore, D. M. (2006). "Earthquake ground-motion prediction equations for eastern North America." *Bull. Seismol. Soc. Am.*, 96(6), 2181–2205.

Bocchini, P., and Frangopol, D. M. (2012). "Restoration of bridge networks after an earthquake: Multicriteria intervention optimization." *Earthquake Spectra*, 28(2), 426–455.

Bruneau, M., et al. (2003). "A framework to quantitatively assess and enhance the seismic resilience of communities." *Earthquake Spectra*, 19(4), 733–752.

Building Seismic Safety Council. (2003). "The 2003 NEHRP recommended provisions for new buildings and other structures. Part 1: Provisions." *FEMA 450*, Washington, DC.

Campbell, K. W. (2003). "Prediction of strong ground motion using the hybrid empirical method and its use in the development of ground-motion (attenuation) relations in eastern North America." *Bull. Seismol. Soc. Am.*, 93(3), 1012–1033.

Chang, S. E., and Shinozuka, M. (2004). "Measuring improvements in the disaster resilience of communities." *Earthquake Spectra*, 20(3), 739–755.

CPLEX [Computer software]. IBM, New York.

Dudenhoeffer, D. D., May, R. P., and Milos, M. (2006). "CIMS: A framework for infrastructure interdependency modeling and analysis." *Proc., 38th Conf. on Winter Simulation*, L. F. Perrone, F. P. Wieland, J. Liu, B. G. Lawson, D. M. Nicol, and R. M. Fujimoto, eds., IEEE, New York, 478–485.

Dueñas-Osorio, L., Craig, J. I., Goodno, B. J., and Bostrom, A. (2007). "Interdependent response of networked systems." *J. Infrastruct. Syst.*, 10.1061/(ASCE)1076-0342(2007)13:3(185), 185–194.

FEMA/NIBS (National Institute of Building Sciences). (2003). *Multi-hazard loss estimation methodology earthquake model (HAZUS-MH MR4): Technical manual*, Washington, DC.

Goda, K., and Hong, H. P. (2008). "Estimation of seismic loss for spatially distributed buildings." *Earthquake Spectra*, 24(4), 889–910.

González, A. D., Dueñas-Osorio, L., Sánchez-Silva, M., and Medaglia, A. L. (2016). "The interdependent network design problem for optimal infrastructure system restoration." *Comput.-Aided Civil Infrastruct. Eng.*, 31(5), 334–350.

Gurobi [Computer software]. Gurobi Optimization, Houston.

Haimes, Y. Y., Horowitz, B. M., Lambert, J. H., Santos, J. R., Crowther, K., and Lian, C. (2005a). "Inoperability input-output model for interdependent infrastructure sectors. II: Case studies." *J. Infrastruct. Syst.*, 10.1061/(ASCE)1076-0342(2005)11:2(80), 80–92.

Haimes, Y. Y., Horowitz, B. M., Lambert, J. H., Santos, J. R., Lian, C., and Crowther, K. G. (2005b). "Inoperability input-output model for interdependent infrastructure sectors. I: Theory and methodology." *J. Infrastruct. Syst.*, 10.1061/(ASCE)1076-0342(2005)11:2(67), 67–79.

Haimes, Y. Y., and Jiang, P. (2001). "Leontief-based model of risk in complex interconnected infrastructures." *J. Infrastruct. Syst.*, 10.1061/(ASCE)1076-0342(2001)7:1(1), 1–12.

IN-CORE. (2017). "Innovative software and data analysis." ⟨https://ssa.ncsa.illinois.edu/isda/projects/in-core/⟩ (Oct. 1, 2017).

Jayaram, N., and Baker, J. W. (2009). "Correlation model for spatially distributed ground-motion intensities." *Earthquake Eng. Struct. Dyn.* 38(15), 1687–1708.

Lee, E. E., Mitchell, J. E., and Wallace, W. A. (2007). "Restoration of services in interdependent infrastructure systems: A network flows approach." *IEEE Trans. Syst. Man Cybern. Part C Appl. Rev.*, 37(6), 1303–1317.

Lin, P., and Wang, N. (2016). "Building portfolio fragility functions to support scalable community resilience assessment." *Sustainable Resilient Infrastruct.*, 1(3–4), 108–122.

Lin, P., and Wang, N. (2017a). "Stochastic post-disaster functionality recovery of community building portfolios. I: Modeling." *Struct. Saf.*, 69, 96–105.

Lin, P., and Wang, N. (2017b). "Stochastic post-disaster functionality recovery of community building portfolios. II: Application." *Struct. Saf.*, 69, 106–117.

Lounis, Z., and McAllister, T. P. (2016). "Risk-based decision making for sustainable and resilient infrastructure systems." *J. Struct. Eng.*, 10.1061/(ASCE)ST.1943-541X.0001545, F4016005.

Luiijf, E., Nieuwenhuijs, A., Klaver, M., van Eeten, M., and Cruz, E. (2008). "Empirical findings on critical infrastructure dependencies in Europe." *Int. Workshop on Critical Information Infrastructures Security*, Springer, Berlin, 302–310.

Mendonça, D., and Wallace, W. A. (2006). "Impacts of the 2001 World Trade Center attack on New York City critical infrastructures." *J. Infrastruct. Syst.*, 10.1061/(ASCE)1076-0342(2006)12:4(260), 260–270.

NIST. (2015). *Community resilience planning guide for buildings and infrastructure systems*, Vols. 1 and 2, Gaithersburg, MD.

Oaks, D. S. (1990). "The damage assessment process: The application of ATC-20." *The Loma Prieta earthquake, studies of short-term impacts*, Institute of Behavioral Science, Boulder, CO.

OSSPAC (Oregon Seismic Safety Policy Advisory Commission). (2013). "The Oregon resilience plan: Reducing risk and improving recovery for the next Cascadia earthquake and tsunami." *Rep. to the 77th Legislative Assembly*, Salem, OR.

Ouyang, M. (2014). "Review on modeling and simulation of interdependent critical infrastructure systems." *Reliab. Eng. Syst. Saf.*, 121, 43–60.

Ouyang, M., and Dueñas-Osorio, L. (2011). "An approach to design interface topologies across interdependent urban infrastructure systems." *Reliab. Eng. Syst. Saf.*, 96(11), 1462–1473.

Poland, C. D. (2013). "Roundtable on standards for disaster resilience for buildings and infrastructure systems." *SPUR resilient city goals*, SPUR, San Francisco.

Rinaldi, S. M., James, P. P., and Terrence, K. K. (2001). "Identifying, understanding, and analyzing critical infrastructure interdependencies." *IEEE Control Syst.*, 21(6), 11–25.

Santos, J. R., and Haimes, Y. Y. (2004). "Modeling the demand reduction input-output (I-O) inoperability due to terrorism of interconnected infrastructures." *Risk Anal.*, 24(6), 1437–1451.

Shinozuka, M., Dong, X., Chen, T. C., and Jin, X. (2007). "Seismic performance of electric transmission network under component failures." *Earthquake Eng. Struct. Dyn.*, 36(2), 227–244.

Steelman, J., Song, J., and Hajjar, J. (2007). "Integrated data flow and risk aggregation for consequence-based risk management of seismic regional loss." *Rep. of the Mid-America Earthquake Center*, Univ. of Illinois at Urbana-Champaign, Champaign, IL.

Trucco, P., Cagno, E., and De Ambroggi, M. (2012). "Dynamic functional modelling of vulnerability and interoperability of critical infrastructures." *Reliab. Eng. Syst. Saf.*, 105, 51–63.

U.S. Geological Survey. (2017). "Seismic hazard maps and site: Specific data." ⟨https://earthquake.usgs.gov/hazards/interactive/⟩ (Oct. 4, 2017).

Utne, I. B., Hokstad, P., and Vatn, J. (2011). "A method for risk modeling of interdependencies in critical infrastructures." *Reliab. Eng. Syst. Saf.* 96(6), 671–678.

Wang, M., and Takada, T. (2005). "Macrospatial correlation model of seismic ground motions." *Earthquake Spectra*, 21(4), 1137–1156.

Xu, W., Hong, L., He, L., Wang, S., and Chen, X. (2011). "Supply-driven dynamic inoperability input-output price model for interdependent infrastructure systems." *J. Infrastruct. Syst.*, 10.1061/(ASCE)IS.1943-555X.0000058, 151–162.